Valence-band structure of α-$MoTe_2$ by angular-resolved photoelectron spectroscopy in the constant-final-state mode

Th. Böker, A. Müller, J. Augustin, C. Janowitz, and R. Manzke
Humboldt-Universität zu Berlin, Institut für Physik, Invalidenstrasse 110, 10115 Berlin
(Received 5 June 1998; revised manuscript received 19 March 1999)

In this work a complete valence-band structure of α-$MoTe_2$ using angular-resolved photoelectron spectroscopy (ARPES) with synchrotron radiation is presented. The dispersion along the perpendicular component $\vec{k}_\perp$ of the wave vector is found to be non-negligible for a number of states, especially at higher binding energies. The effect of this $\vec{k}_\perp$ dispersion on the determination of the exact dispersion of the individual states along $\vec{k}_\parallel$ is discussed. By performing ARPES in the constant-final-state mode for off-normal emission spectra, at least the $\vec{k}_\parallel$ component can be determined unequivocally. Comparison of theoretical calculations with the resulting experimental valence-band structure shows partial agreement.
[S0163-1829(99)01131-5]

I. INTRODUCTION

$MoTe_2$ belongs to the large family of layered transition metal dichalcogenides (LTMD) whose crystal structure results from the stacking of sheets of hexagonally packed atoms in the sequence Te-Mo-Te, Te-Mo-Te. *Molybdenum ditelluride* crystallizes in two forms. The so-called β-$MoTe_2$ form or high-temperature modification, stable above 900 °C, has a monoclinic structure and shows metallic conduction behavior[1] similar to WTe_2.[2] The MoS_2 type—also denoted as α-$MoTe_2$—is the polytype stable below $\approx$815 °C. α-$MoTe_2$ is a semiconductor with an indirect band gap of 1.0 eV and a direct optical band gap of 1.1 eV.[3] Since the optical band gap of α-$MoTe_2$ matches well with the solar spectrum, this material is used for electrodes in high efficiency photoelectrochemical (PEC) cells.[4] As in all molybdenum dichalcogenides (i.e., MoS_2, $MoSe_2$, and $MoTe_2$) the phototransitions involve nonbonding *d* orbitals of Mo atoms. Therefore, these materials can be expected to resist hole-induced corrosion.[5] Despite the major importance of α-$MoTe_2$ in solar cell production, no precise band structure determination has been reported yet.

Early photoemission studies on α-$MoTe_2$ show hardly any agreement with theory.[6,7] As will be shown in the present work, the assumption of flat bands in the direction perpendicular to the surface[6] is inaccurate and therefore the band structure needs to be revisited with more accurate experiments. This work supersedes previous measurements by using the constant-final-state (CFS) mode of angular-resolved photoelectron spectroscopy (ARPES) with synchrotron radiation. This is essential, because the spectra recorded at a photon energy of $h\nu = 21.22$ eV (i.e., He $I\alpha$ of helium resonance lamp) in normal emission are close to the *A* point of the Brillouin zone. Consequently one can never reach the Γ point and decide where the valence-band maximum is located.

II. EXPERIMENTAL DETAILS

The 2H polytype of the crystal structure of α-$MoTe_2$ is characterized by a stacking sequence $/AbABaB/$ (A,B: Te atom; b,a: Mo atom).[8] A Mo-atom layer is sandwiched between two Te-atom layers and above the one Te-Mo-Te layer the following Te-Mo-Te layer is shifted such that the Mo atom is directly above a Te atom of the first layer. These layers are held together only by weak van der Waals forces which give rise to the quasi-two-dimensional character of the electronic structure. One unit cell and the corresponding first Brillouin zone are displayed in Fig. 1.

From the lattice parameters, $a = 3.517$ Å and $c = 2 \times 6.981 = 13.962$ Å (Ref. 8) the reciprocal lengths of the high-symmetry lines are as given in Table I.

Single crystals of α-$MoTe_2$ have been grown using the chemical vapor transport method (CVT). We used bromine as the transport agent and therefore the semiconducting character is of *n* type.[9]

Coarse orientation of the samples was achieved by Laue and by low-energy electron diffraction (LEED) patterns. In Fig. 2 a LEED pattern of α-$MoTe_2$ taken with an incident electron energy of $E_{kin} = 84$ eV is shown. As can be concluded from the sharpness of the diffraction pattern, the single crystals are of high quality.

After preadjustment the crystals were cleaved *in situ* by knocking off a small aluminum post which was glued on top of the samples. This was done at *T* equal to room temperature under ultrahigh-vacuum conditions ($p \leqslant 2 \times 10^{-10}$ mbar) to minimize surface degradation or contamination. Immediately after the cleavage a reference spectrum was recorded to check the surface quality from time to time. Even after 40 h of data acquisition at room temperature no

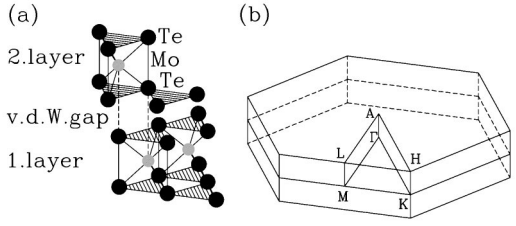

FIG. 1. Crystal structure (a) and the first Brillouin zone (b) of α-$MoTe_2$.

 ©1999 The American Physical Society

TABLE I. Reciprocal lengths of the high-symmetry lines of α-$MoTe_2$.

ΓA	=	0.225 Å^{-1}
ΓM	=	1.030 Å^{-1}
ΓK	=	1.190 Å^{-1}
MK	=	0.595 Å^{-1}

significant changes were observed. This is due to the crystals cleaving at the van der Waals gap, resulting in a rather inert surface.

The measurements have been performed at the synchrotron radiation center HASYLAB in Hamburg, Germany. A 3 m normal incidence monochromator with a photon energy range of $h\nu = 9, \ldots, 30$ eV and a monochromator resolution of about 30 meV has been used at the HONORMI beamline of the storage ring DORIS. The photoelectron spectrometer is a homemade hemispherical deflection analyzer mounted on a two axis goniometer. For the measurements presented here we have chosen a monochromator resolution of 30 meV and an analyzer resolution of 50 meV, yielding an overall resolution of 60 meV.

The entrance optics of the analyzer consists of a four-element electrostatic lens system which can be operated in two different modes. The first is the spatial resolving mode with a constant linear magnification $M_{\mathrm{lin}} = -0.5$. Electrons originating from the object plane, i.e., the sample, with the same start radius with respect to the electro-optical axis but with different angles are focused at the same exit radius on the image plane, i.e., the Herzog plate of the analyzer. By using an entrance aperture 1 mm in diameter, only those electrons that originate within a region of the sample 2 mm in diameter are detected by the analyzer. In this mode, electrons coming from outside the electron optical focus are suppressed.

The other mode is the new angular resolving mode.[10] In this mode the electrons starting from the sample with the same angle but with different radii (with respect to the electro-optical axis) are focused at the same radius at the image plane. Small starting angles are focused closer to the electro-optical axis. The aperture at the image plane allows only those electrons to pass which have a sufficiently small starting angle. The angular resolution is determined by the size of the aperture at the image plane and here a constant angular resolution of better than $\Delta\vartheta \leqslant 0.4°$ is achieved.[10]

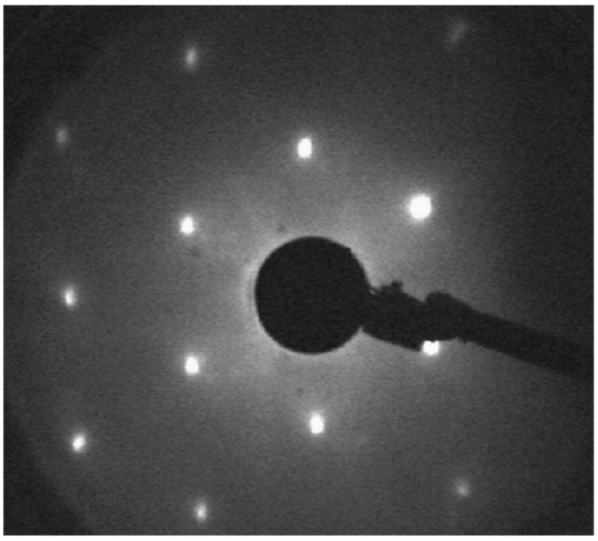

FIG. 2. LEED pattern of α-$MoTe_2$ taken with an incident electron energy of $E_{\mathrm{kin}} = 84$ eV.

Photoemission spectroscopy can be performed in several different modes to determine the occupied band structure. Most common is the energy distribution curve (EDC) mode in which the photon energy is held constant and the detected kinetic energy is varied. With the emission angle ϑ (with respect to the surface normal) and the detected kinetic energy E_{kin} of the photoelectrons the wave-vector component parallel to the planes is determined by the dispersion relation

$$|\vec{k}_{\parallel}| = \frac{1}{\hbar}\sqrt{2m_e E_{\mathrm{kin}}}\sin\vartheta. \tag{1}$$

The $\vec{k}_{\perp}$ component is not conserved as the electron travels through the crystal surface. For many three-dimensional crystals the final state can be well approximated by free-electron parabola:

$$|\vec{k}_{\perp}| = \frac{1}{\hbar}\sqrt{2m_e(E_{\mathrm{kin}}\cos^2\vartheta + V_0)}. \tag{2}$$

This approximation fails, if the final states are not free-electron-like as is the case for the more two-dimensional LTMD's. The inner potential V_0 is characteristic of each sample and recent studies show that it is even dependent on $\vec{k}$.[11,12] Therefore, an accurate determination of the absolute value of $\vec{k}_{\perp}$ for each spectrum along any $\vec{k}_{\parallel}$ direction cannot be performed without explicit knowledge of the shape of the final states. Only for normal emission can the $\vec{k}_{\perp}$ component be determined by the critical points which can be found precisely from the symmetry of the dispersion of the uppermost band along $\overline{\Gamma A \Gamma}$. Furthermore, the critical points at the Brillouin zone edge can be found also, but the $\vec{k}_{\perp}$ component remains undetermined. This is not critical, since all valence bands show negligible dispersion in the direction perpendicular to the planes at the zone edge and an accurate determination of the $\vec{k}_{\perp}$ component near the zone edges is not necessary.

Equations (1) and (2) show that both $\vec{k}$ components depend on the kinetic energy. Therefore, the emission features in an EDC spectrum are affected by a dispersion in both directions. For a strong dispersing band the corresponding peaks appear asymmetric within the EDC spectra. The former can be circumvented in the constant-final-state mode where both $\vec{k}$ components ($\vec{k}_{\parallel}$ and $\vec{k}_{\perp}$) are kept constant. A spectrum at a new value of e.g., $\vec{k}_{\parallel}$, is adjusted by choosing a couple $(E_{\mathrm{kin}}, \vartheta)$ for which $\vec{k}_{\perp}$ remains constant. The $\vec{k}_{\perp}$ component is calculated from Eq. (2), but the resulting value cannot be taken to determine the exact position within the Brillouin zone. It is only a value from which together with Eq. (1) the couple $(E_{\mathrm{kin}}, \vartheta)$ is calculated. The range of these values is limited by the monochromator energy range so that not all high-symmetry directions were accessible. All mea-

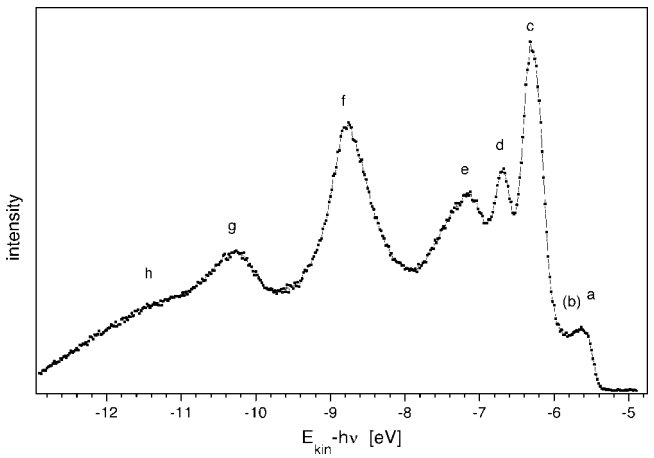

FIG. 3. Energy distribution curve at the Γ point ($h\nu = 15.75$ eV) with assignment of the emission features (see text).

surements have been performed with an overall resolution of about 60 meV and a maximum acceptance angle of the photoelectrons of $\Delta\vartheta \pm 1.05°$.

III. RESULTS AND DISCUSSION

We assign ϑ as the polar and φ as the azimuthal angle with respect to the surface normal. The surface normal (ϑ_0, φ_0) is found by using the symmetry of ARPES spectra along high-symmetry directions. Since the upper valence bands show significant dispersion, this adjustment is very accurate. The spectrum at the Γ point is displayed in Fig. 3 ($h\nu = 15.75$ eV) and for the sake of clear notation, all emission features were assigned alphabetically.

In order to investigate the dependence of the dispersion of the bands perpendicular to the cleavage plane, the first spectra series was been recorded at normal emission ($\vartheta = 0°$) for varying photon energies [see Fig. 5(a)]. The spectra were lined up by a standard technique of photoemission on semiconductors given by, e.g., Ref. 13. Explicitly, the energy axis of all spectra in common has been related to the valence-band maximum (VBM), so it is given in binding energy. All spectra remain at the same energetic position relative to each other and therefore the dispersions are not caused by mathematical treatment. The charging of the sample can be detected by irradiating the sample with different photon fluxes, leading to an energy shift of the emission features. None was observed within the experimental accuracy.

For a precise determination of the peak positions we used a curve fitting program based on the Levenberg-Marquardt algorithm.[14] The model function is created by convoluting a sum of peaks plus Shirley background[15] with the Gaussian shaped spectrometer function. Emission features $c-h$ have a Lorentzian line shape which is in agreement with the physical nature of the electronic states. The topmost peak is asymmetric and its line shape could not be clarified yet. Therefore it is approximated by a sum of two Gaussian-like line shapes a and (b). In the following only the energetic peak position of peak a, which is the maximum of the observed asymmetric emission feature, is used.

A close look at the topmost emission feature (i.e., a) of Fig. 5(a) reveals a weak but clear photon energy dependent dispersion. The kinetic energy with respect to the photon

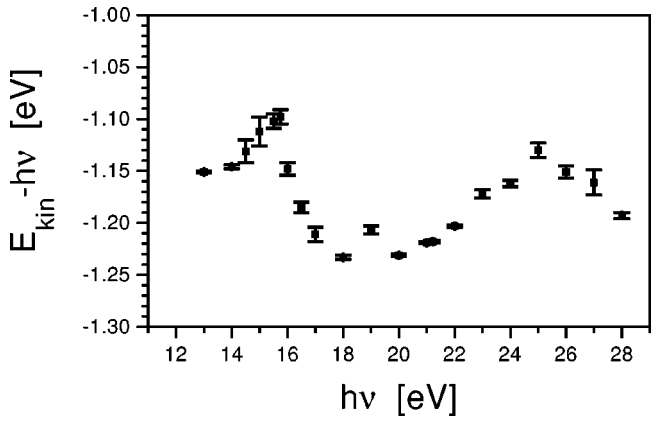

FIG. 4. Dispersion of the topmost emission feature a of Fig. 3 from the photon energy dependent spectra series perpendicular to the cleavage plane ($\vartheta = 0°$) shown in Fig. 5(a).

energy of this peak is plotted in Fig. 4. Clearly, two maxima are visible at $h\nu = 15.75$ eV and $h\nu = 26$ eV which correspond to high-symmetry points of the Brillouin zone. In accordance with the similar band structures along ΓA of $MoSe_2$ and MoS_2 (Ref. 16), they are related to Γ points. With the reciprocal length of $\Gamma A\Gamma = 0.45$ Å^{-1} and by using Eq. (2), a median inner potential V_0 thus obtained is 14 ± 1 eV. Again we denote that this value can vary by about 2–3 eV with $\vec{k}$ according to Ref. 11.

Apart from strong intensity modulations due to photon energy dependent transition probabilities, strongly dispersive peaks are observed in Fig. 5(a) about -1.2 eV below the valence-band maximum. These can be ascribed to bonding Te $5p_z$ orbitals since they are oriented out of plane.[17] McGovern and co-workers[18,6] carried out photoelectron spectroscopy in the EDC mode on α-$MoTe_2$ and assumed flat bands in the direction perpendicular to the plane (ΓA direction). They concluded that due to the complexity of the band structure and the emission process, the information relating to the band structure cannot be extracted from ARPES.[6] We found that their $\vec{k}_\parallel$ band structure is a combination of the dispersions in the $\vec{k}_\parallel$ and $\vec{k}_\perp$ directions. Despite a minor dispersion of the bands in the direction perpendicular to the planes in comparison to the dispersion along $\vec{k}_\parallel$, influence on their EDC spectra by asymmetric emission features is clearly observed. To ensure that (in our data) all measured states $E(\vec{k})$ are unaffected by a dispersion within a spectrum, all other spectra are recorded in the CFS mode. As pointed out in the section above, in this mode the $\vec{k}_\parallel$ and $\vec{k}_\perp$ components are held constant. The resulting spectra were more easily fitted due to the absence of asymmetric emission features, except for features a and (b).

From the spectra along the ΓA, $\Gamma K(H)$, $MK(LH)$, and $\Gamma M(L)$ directions shown in Figs. 5 and 6, it was easy to determine the complete detailed valence-band structure, since the spectra show sharp features due to the enhanced energy and angular resolution compared to the previous measurements. Again, the spectra were lined up by the standard technique of photoemission on semiconductors mentioned above.

Figure 7 shows the complete valence-band structure along the high-symmetry directions $\Gamma M(L)$, $MK(LH)$, $\Gamma K(H)$,

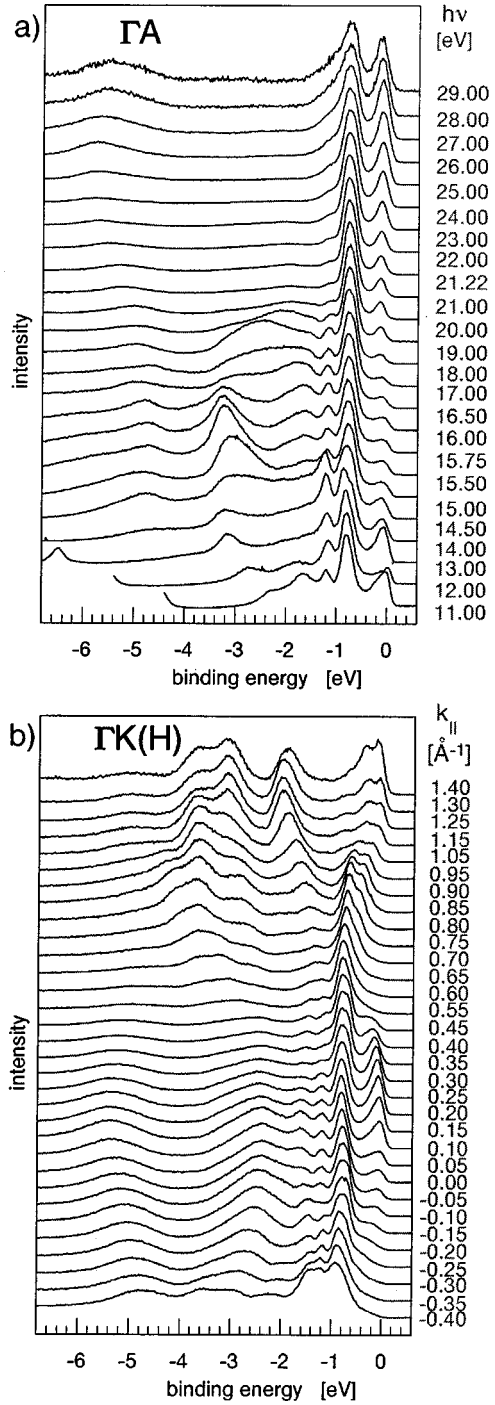

FIG. 5. (a) Spectra series in the ΓA direction (EDC) and (b) spectra series in the $\Gamma K(H)$ direction (CFS).

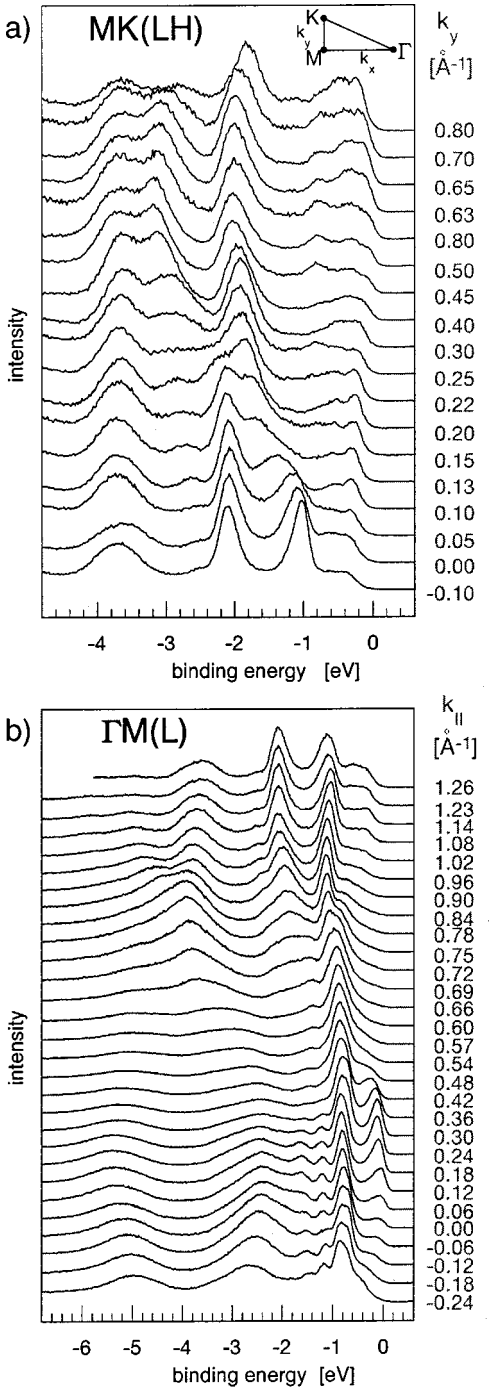

FIG. 6. (a) Spectra series in the $MK(LH)$ direction (CFS) and (b) spectra series in the $\Gamma M(L)$ direction (CFS).

and ΓA. The binding energy error bars are the statistical errors of the fitted peak positions while the error bars on the $\vec{k}$ axis result from the acceptance angle $\Delta\vartheta \pm 1.05°$ of the spectrometer.

A. Valence-band structure

The schematic band model for the density of states (DOS) is depicted in Fig. 8 for the case of MoS_2.[19] It is generally accepted that the valence bands consist of Mo $4d$ and chalcogen p/d states.[8] McGovern and Williams have shown that for α-$MoTe_2$ the strongest emission feature in the valence-band spectra near the Γ point (peak c in our data) is derived from wave functions having d_{z^2} symmetry.[18] The energetic position of this state with respect to the VBM and the dispersion of the Te p/d states will be treated in the following.

The valence-band maximum is found at the Γ point, in agreement with similar studies on MoS_2 and $MoSe_2$.[20] (For convenience, we assign the energy position of the maximum of the uppermost emission feature a as the valence-band maximum.) According to the band structure calculations for this class of materials, the character of the two topmost emission features $a(b)$ is a mixing of Mo $4d$ with Te $5p$ orbitals. About halfway from Γ to $K(H)$ or Γ to $M(L)$, respectively,

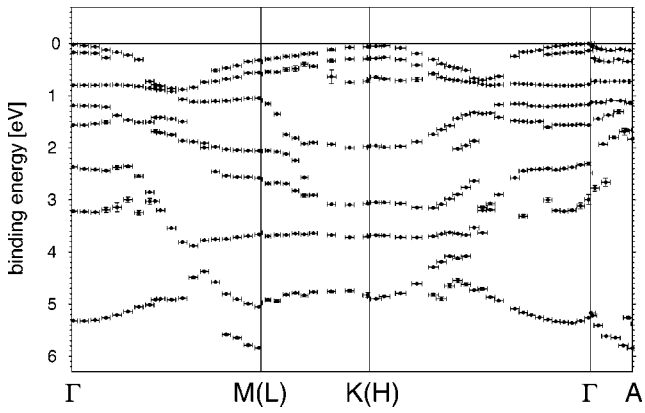

FIG. 7. Experimental valence-band structure of α-$MoTe_2$ derived from the spectra series along the ΓA, $\Gamma K(H)$, $MK(LH)$, and $\Gamma M(L)$ directions.

these states disperse to higher binding energies and merge into emission feature *c*. The latter is predominantly of Mo $4d_{z^2}$ character[18] and has only about 150 meV $\vec{k}_{\|}$ dispersion towards the Brillouin zone edge. For $MoSe_2$ an equivalent, rather dispersionless state has been reported[16] and discussed in the context of a vibronic polaron similar to the electronic polaron claimed for $TiTe_2$.[21] Very recent studies[17] on $TiTe_2$ disprove the electronic polaron concept so that also in the case of similar LTMD's other explanations may be more plausible. We suggest peak *c* to be nondispersive simply due to a weak overlap of the Mo $4d_{z^2}$ orbital with other orbitals in the direction close to the *z* axis. With increasing off-normal emission angles ϑ, i.e., reaching the Brillouin zone edge, the small overlap with the Te $5p_z$ orbital gives rise to the observed dispersion. Since the Mo $4d_{z^2}$ orbital is fully occupied, high spectral intensity of this emission feature for small emission angles ϑ is found which is decreasing for increasing ϑ due to a shielding by the Te $5p_z$ orbitals.

In the spectra series along the $\Gamma K(H)$ symmetry line shown in Fig. 6(b), a double emission feature appears near

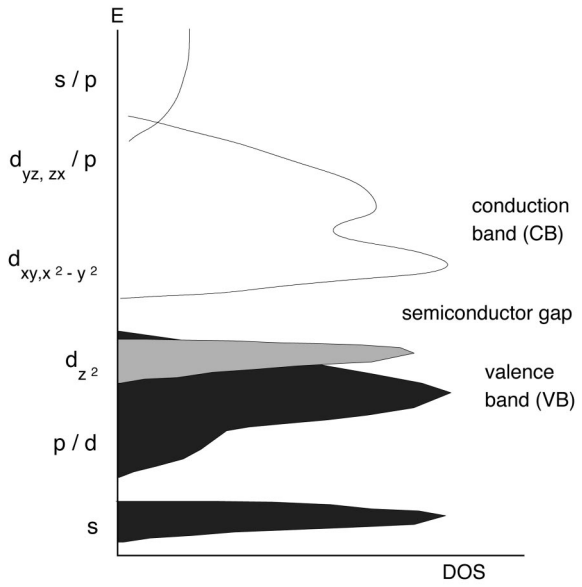

FIG. 8. Schematic band model for the densitiy of states (DOS) of MoS_2 ($c/a = 3.89$). Redrawn after Friend and Yoffe (Ref. 19).

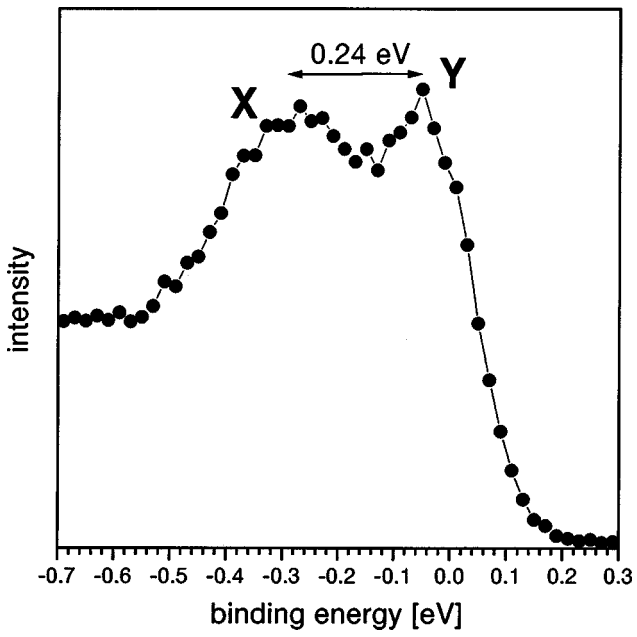

FIG. 9. Double emission feature at the $K(H)$ point of the Brillouin zone (for assignments see text).

the VBM in the vicinity of the $K(H)$ point of the Brillouin zone with a splitting of ≈ 0.24 eV (see Fig. 9). As claimed by Coehoorn, Haas, and de Groot,[20] who observed a splitting of 0.21 eV for $MoSe_2$ at the $K(H)$ point, these states give rise to the excitonic features *A* and *B* known from optical absorption data (see, e.g., Ref. 22). The splitting for $MoSe_2$ matches well with the observed energetic difference of the excitons *A* and *B* (see, e.g., Ref. 23) and therefore they concluded that the exciton peaks probably arise from transitions at the $K(H)$ point. This is in contrast to several investigations using optical absorption measurements[24,22,25] which led to the result that appropriate transitions for the *A*, *B* excitons should occur at the Γ point. However, according to our data the peak distance of ≈ 0.24 eV for the double feature *X*, *Y* at the $K(H)$ point for $MoTe_2$ is much too small compared to the 0.38 eV distance of the excitonic lines measured by Beal, Knights, and Liang.[22] Even though a shift between the initial states and the observed energy distance of the excitons is possible,[26] the magnitude of the observed shift cannot be explained within the theory.[26] We conclude accordingly that the double emission feature *X*, *Y* at the $K(H)$ point does not correspond to *initial states* of the excitons *A* and *B*. In line with optical absorption measurements of Refs. 24, 22, and 25 and from the location of the VBM at the Γ point, we suggest the topmost occupied state at Γ to be the initial state for the *A*, *B* excitons.

The c/a ratio is an important quantity in determining the position of the Mo $4d_{z^2}$ band.[19] To be precise, the d_{z^2} band is shifted towards higher binding energies with increasing c/a ratio. Since α-$MoTe_2$ has the largest c/a ratio, i.e., $c/a = 3.968$ (Ref. 8) compared to the other members of the MoX_2 family [i.e., 3.890 for MoS_2 and 3.924 for $MoSe_2$ (Ref. 8)], the d_{z^2} emission feature (*c*) should have the highest binding energy. Indeed, we found this peak to be located about 0.8 eV below the valence-band maximum while a value of 0.4 eV has been reported in the case of $MoSe_2$.[16] For MoS_2 recent studies[27] show the dispersion of bands in

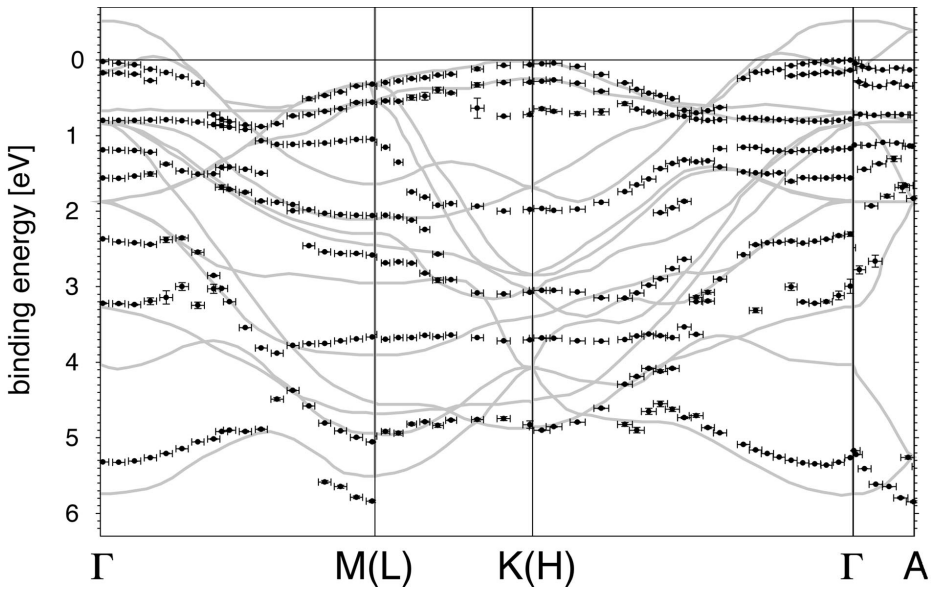

FIG. 10. Experimental valence-band structure of α-$MoTe_2$ in comparison with a calculation for $MoSe_2$ using the scalar relativistic ASW method (Ref. 16).

normal emission to be also non-negligible. An experimental band structure investigation including the issue of the location of the Mo $4d_{z^2}$ band is in preparation.[27]

B. Comparison with theoretical band structures

To our knowledge there exist three theoretical calculations for α-$MoTe_2$ which differ remarkably. Bromley, Murray, and Yoffe used the semiempirical tight binding method in two dimensions.[25] The tendencies in the upper valence bands seem to be comparable to our experimental data, but the lower lying bands differ. This disagreement is mainly due to the fact that the dispersion in the $\vec{k}_\perp$ direction is neglected. In addition to that, they found the valence-band maximum at the K point in contrast to our data. Finally the calculated bandwidth of about 4.2 eV is much too small compared to the measured bandwidth of 6.0 eV.

Dawson and Bullet calculated the band structure by applying an *ab initio* linear combination of atomic orbitals (LCAO) method.[28] They found the VBM to be at the M point of the Brillouin zone, which differs completely from our data. Second, the calculated bandwidth of about 7.3 eV is much larger than in any other band structure of the MoX_2 family (see, e.g., Ref. 20) and is significantly larger than in our measurements.

A slightly better agreement is achieved by the calculation of Hindt and Lee, who used the Korringa-Kohn-Rostoker (KKR) method.[29] Despite the poor correspondence of the lower-lying bands, the trends of the upper bands agree partially with our experimental data. Especially the VBM is at the same location (Γ point) and the calculated bandwidth of about 6.8 eV is only 800 meV wider than found experimentally. Note that the number of bands is inconsistent in this calculation (seven bands at Γ point of the $\overline{\Gamma M}$ direction and eight bands at the Γ point of the $\overline{\Gamma A}$ direction).

Tight binding (=LCAO) methods can be characterized as a model of isolated atoms with interaction. Due to this ansatz they are well suited to inhomogeneous systems including defects and surfaces. The more sophisticated muffin tin methods, such as KKR and augmented plane wave (APW), work with wave functions that are atomiclike at the cores and plane-wave-like in between. These wave functions can be regarded as being very close to the real crystal wave functions and therefore deliver more realistic results. Common to all calculations is that they neglect spin-orbit splitting. In our data this splitting is clearly visible at the $K(H)$ point.

For $MoSe_2$ an augmented-spherical-wave (ASW) method including scalar relativistic effects which shows good correspondence to experiment has been reported.[16] A direct comparison of our experimental data with the ASW calculation for the isoelectronic $MoSe_2$ taken from Ref. 16 is shown in Fig. 10. The energy axis has been shrunk by a factor to get the best correspondence, since $MoSe_2$ is expected to have a larger bandwidth compared to $MoTe_2$. Furthermore, the theoretical calculation has been aligned with the experimental data at the $K(H)$ point since this shows the best correspondence. However, the courses of the bands are in good agreement while the energetic position is different. Especially the magnitude of the spin-orbit splitting at the $K(H)$ point is very similar. Such band structure calculations for $MoTe_2$ have to be done to yield better agreement with the experimental data.[30]

ACKNOWLEDGMENT

We would like to thank D. Kaiser for assistance in the crystal fabrication. This work received funding from the Bundesministerium für Bildung, Wissenschaft, Forschung und Technologie (BMBF) under Project No. 05 622 KHA.

[1] R. M. A. Lieth and J. C. J. M. Terhell, *Preparation and Crystal Growth of Materials with Layered Structures* (D. Reidel Publishing Company, Dordrecht, 1977), p. 141.
[2] J. Augustin, V. Eyert, Th. Böker, C. Janowitz, and R. Manzke, (unpublished).
[3] A. J. Grant, T. M. Griffiths, G. D. Pitt, and A. D. Yoffe, J. Phys. C **8**, L17 (1975).
[4] H. D. Abruña, G. A. Hope, and A. J. Bard, J. Electrochem. Soc. **129**, 2224 (1982).
[5] M. Kettaf, A. Conan, A. Bonnet, and J. C. Bernede, J. Phys. Chem. Solids **51**, 333 (1990).
[6] I. T. McGovern, R. H. Williams, and A. W. Parke, J. Phys. C **12**, 2689 (1979).
[7] R. Manzke and M. Skibowski, in *Electronic Structure of Solids: Photoemission Spectra and Related Data*, edited by A. Goldmann, Landolt-Börnstein, New Series, Group III, Vol. 23, pt. B (Springer-Verlag, Berlin, 1994), p. 140.
[8] J. A. Wilson and A. D. Yoffe, Adv. Phys. **18**, 193 (1969).
[9] A. Conan, A. Bonnet, A. Amrouche, and M. Spiesser, J. Phys. (France) **45**, 459 (1984).
[10] Th. Böker, A. Müller, J. Brügmann, J. Wichert, W. Frentrup, C. Janowitz, and R. Manzke, J. Electron Spectrosc. Relat. Phenom. **87**, 195 (1998).
[11] V. N. Strocov, H. I. Starnberg, P. O. Nilsson, H. E. Bauer, and L. J. Holleboom, J. Phys.: Condens. Matter **10**, 5749 (1998).
[12] V. N. Strocov, H. I. Starnberg, P. O. Nilsson, H. E. Bauer, and L. J. Holleboom, J. Phys.: Condens. Matter **8**, 7539 (1996).
[13] *Photoemission in Solids I: General Principles*, edited by M. Cardona and L. Ley, Topics in Applied Physics Vol. 26 (Springer-Verlag, Berlin, 1979).
[14] W. H. Press, S. A. Teukolsky, W. T. Vetterling, and B. P. Flannery, *Numerical Recipes in C*, 2nd ed. (Cambridge University Press, Cambridge, England, 1992).
[15] D. A. Shirley, Phys. Rev. B **5**, 4709 (1972).
[16] R. Coehoorn, C. Haas, J. Dijkstra, C. J. F. Flipse, R. A. de Groot, and A. Wold, Phys. Rev. B **35**, 6195 (1987).
[17] R. Claessen, R. O. Anderson, G.-H. Gweon, J. W. Allen, W. P. Ellis, C. Janowitz, C. G. Olson, Z. X. Shen, V. Eyert, M. Skibowski, K. Friemelt, E. Bucher, and S. Hüfner, Phys. Rev. B **54**, 2453 (1996).
[18] I. T. McGovern and R. H. Williams, Nuovo Cimento B **38**, 241 (1977).
[19] R. H. Friend and A. D. Yoffe, Adv. Phys. **36**, 1 (1987).
[20] R. Coehoorn, C. Haas, and R. A. de Groot, Phys. Rev. B **35**, 6203 (1987).
[21] D. K. G. de Boer, C. F. van Bruggen, G. W. Bus, R. Coehoorn, C. Haas, G. A. Sawatzky, H. W. Myron, D. Norman, and H. Padmore, Phys. Rev. B **29**, 6797 (1984).
[22] A. R. Beal, J. C. Knights, and W. Y. Liang, J. Phys. C **5**, 3540 (1972).
[23] A. R. Beal, W. Y. Liang, and H. P. Hughes, J. Phys. C **9**, 2449 (1976).
[24] M. Tanaka, H. Fukutani, and G. Kuwabara, J. Phys. Soc. Jpn. **456**, 1899 (1978).
[25] R. A. Bromley, R. B. Murray, and A. D. Yoffe, J. Phys. C **5**, 759 (1972).
[26] Y. Onodera and Y. Toyozawa, J. Phys. Soc. Jpn. **223**, 1601 (1967).
[27] Th. Böker, C. Janowitz, and R. Manzke (unpubished).
[28] W. G. Dawson and D. W. Bullet, J. Phys. C **20**, 6159 (1987).
[29] S. P. Hindt and P. M. Lee, J. Phys. C **13**, 349 (1980).
[30] I. T. McGovern and R. H. Williams, J. Phys. C **9**, L337 (1976).